Quantum Tunneling Sb-Heterostructure Millimeter-Wave Diodes

J. N. Schulman, E. T. Croke, D. H. Chow, H. L. Dunlap, K. S. Holabird
HRL Laboratories, Malibu, CA

M. A. Morgan, S. Weinreb
California Institute of Technology, Pasadena, CA

ABSTRACT

We have developed a new zero bias millimeter wave diode based on quantum tunneling in an InAs/AlSb/GaSb nanostructure. It is ideal for square law radiometry and passive millimeter wave imaging. Excellent sensitivity has been demonstrated at present up to 110 GHz, with higher bandwidth predicted for smaller area diodes.

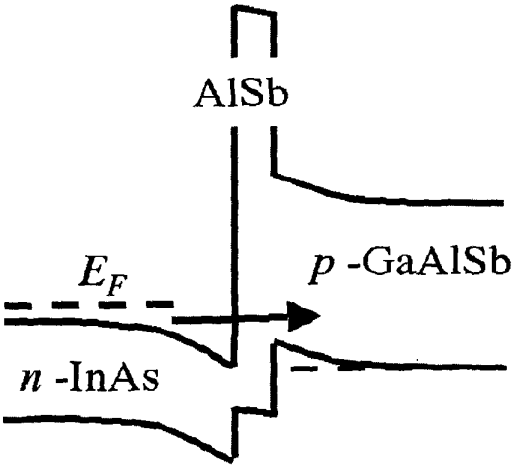

Figure 1. Schematic band edge diagram of InAs/AlSb/GaAlSb heterojunction in forward bias.

INTRODUCTION

We have recently proposed a new type of millimeter wave diode based on epitaxial layers of the InAs/AlSb/GaSb family of nearly-lattice matched III-V semiconductors [1]. The principal of operation is similar to that of an Esaki backward diode in that the controlling current mechanism is interband tunneling between adjacent energetically offset semiconductor regions. The Type II band gap line-up between InAs and GaSb, where the conduction band minimum of InAs lies energetically below the valence band maximum of GaSb, creates a natural asymmetry in the current flow with bias direction, Fig. 1. Forward bias current is low because the conduction band electrons from the InAs are blocked by the GaAlSb band gap. Backward bias current is large due to GaAlSb valence electrons flowing freely into the InAs conduction band. The resulting curvature in the I(V) characteristic is ideal for zero bias direct detection, or mixing with low local oscillator power [2]. Previously reported DC characteristics were promising, especially the high curvature coefficient and relatively low junction resistance, but the high frequency performance was yet to be ascertained. In this paper we present the results of S-parameter and voltage sensitivity measurements from 1 to 110 GHz. They show that diodes with 2x2 μm^2 area have excellent response at 110 GHz, and higher frequencies should be achievable with smaller areas.

SAMPLES

The basic structure of the diodes was described previously [1]. There is great flexibility in the design parameters available, and we have only begun to explore the design space. The device can be grown on lattice matched or mismatched substrates including GaAs and InP. In this it is similar to resonant interband tunneling devices that we have grown and that have been monolithically integrated with InP-based high electron mobility transistors [3]. At this time we have standardized on a family of structures that have the layer design, doping, alloy concentrations, and layer widths of sample SB2407 [1]. SB2407 had a nominal AlSb barrier thickness of 20Å. We have grown a series of similar samples but with the AlSb thickness varied from 20 to 50Å. The main effect of the barrier thickness is in controlling the magnitude of the tunneling current, as seen in the video resistance R_V. We have plotted R_V, as determined from the slope of the DC I(V) curve at zero bias, versus AlSb barrier thickness in Fig. 2. In the simplest model ignoring series resistance, R_V should exponentially increase as the thickness increases. Figure 2 confirms this and also illustrates the reproducibility and control of the MBE process for this purpose. The data points are all reasonably close to the fit represented by the solid line, even though the samples were grown over a several month period and in-situ monitoring and feedback techniques were not employed. This is of great benefit for imaging array applications where reproducibility and uniformity can greatly simplify design and reduce cost. Note that the fit extrapolates to less than 200 $\Omega \cdot \mu m^2$ for L_B=10Å.

The voltage sensitivity is the DC voltage out from the diode per power reaching it. It is proportional to the curvature coefficient, $\gamma = d^2I/dV^2/(dI/dV)$, which should be as large as possible. We have found that γ is only weakly dependent on barrier thickness, but that there is a noticeable dependence on growth order as follows. The samples numbered below (SB)2700 in Fig. 2 were grown in the order Substrate/InAs/AlSb/GaAlSb/GaSb/InAs [1]. The curvature coefficients were 16.2, 17.8, and 19.6/Volt for the three 20Å

barrier thickness cases, and 20.7 and 21.7/Volt for the 25Å and 30Å cases, respectively. The layers for the four samples 2717, 2774, 2775, and 2776 were all grown in the reverse order. Their curvature coefficients were significantly larger, 27.5 and 27.4/Volt for the two 30Å barrier samples, and 28.0 and 29.3/Volt for the 40Å and 50Å samples. We do not have an explanation for this effect, but it is well known that the growth order as well as the precise chemical nature of the non-common anion interface affect several of the electrical and optical properties [4].

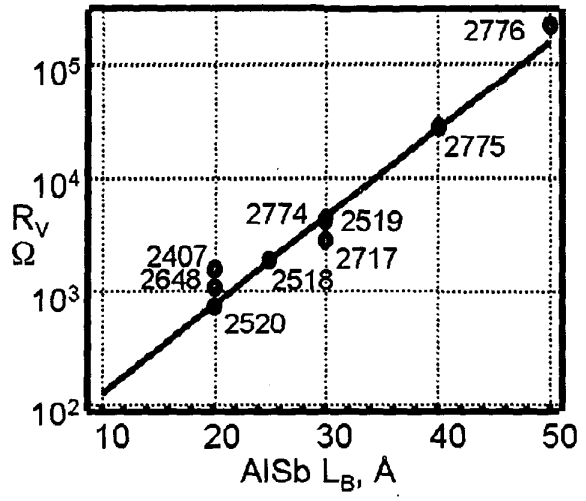

Figure 2. Diode video resistance, dV/dI, determined from the slope of the DC I(V) curves at zero bias versus AlSb barrier thickness.

MEASUREMENTS

We present the high frequency measurement results in detail for one particular diode, SB2775, for four device cross-sectional areas in Table 1. The diodes were tested below 50 GHz with a vector network analyzer and probe station. The power delivered to the chip was between 0.3 and 1.2 μW. For higher frequency impedance measurements an Oleson WR-8 VNA extension was used with the network analyzer. To avoid spurious tones a backward wave oscillator was employed for the higher frequency sensitivity data.

TABLE I
S-PARAMETER FIT, DIODE IMPEDANCE AND SENSITIVITY

Area μm^2 (#)	C_P fF (fit)	R_S Ω (fit)	R_J Ω (fit)	C_J fF (fit)	Z_D Ω 95 GHz	β_V V/W 95 GHz	$\beta_{V,opt}$ V/W 95 GHz
2x2(a)	6	63	9567	11	26.2-j92.4	2768	7576
2x2(b)	6	69	13204	11	30.2-j91.0	2664	6483
3x4(a)	17	11	2249	39	8.28-j23.2	750	1781
3x4(b)	17	11	2284	37	8.14-j23.1	837	2013
4x4(a)	22	9	1542	57	6.19-j13.6	336	907
4x4(b)	22	10	1460	57	6.57-j13.0	385	986
5x5(a)	31	7	805	103	4.62-j6.00	101	331
5x5(b)	31	7	781	97	4.83-j5.98	106	333

The diode small-signal equivalent circuit used for this analysis is shown in the inset to Figure 3. The package capacitance, C_P, was estimated numerically from the diode geometry. A nominal value of L_P=20 pH was determined for the lead inductance as a best fit to the data. R_J was calculated as the ratio of the open-circuit voltage and short-circuit current produced in the diode under RF drive. This method was considered to be more accurate than extraction from the S-parameter measurements, given the typically large values of R_J compared to 50 Ω. The geometric trend in R_J revealed that the smallest diodes, drawn as 2x2 μm^2, came out smaller after fabrication. The data suggest that they are closer to about 3 μm^2 in size and are less uniform.

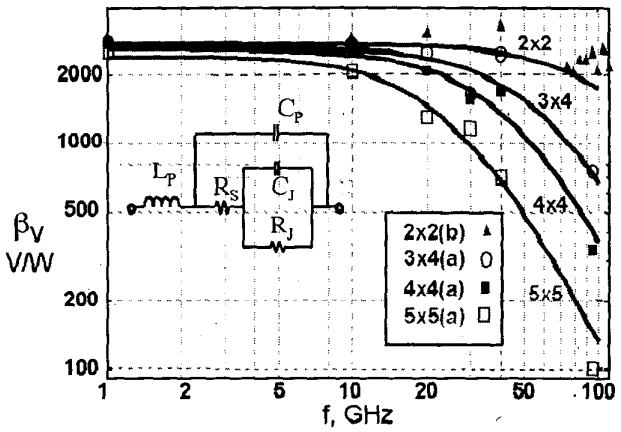

Figure 3. Measured unmatched voltage sensitivity of SB2775 versus frequency. Inset is diode circuit model.

The remaining two parameters, R_S and C_J, were calculated for each frequency from the data. The calculation was most reliable at the higher frequencies where the reactance of C_J was not too large. The final parameter values are those obtained at 95 GHz for the 2x2 μm^2 diodes, and the average of those obtained at 30, 40, and 95 GHz for the other diodes. The measured voltage sensitivity, β_V, was determined as the open-circuit DC voltage divided by the incident RF power.

The results of the diode model parameter fitting are listed in Table 1, with the 95 GHz diode impedances and sensitivities. We compared the measured sensitivity to a simple model as follows. The optimal, perfectly matched sensitivity and the measured sensitivity are related by $\beta_V = \beta_{V,opt}\left(1-|S_{11}|^2\right)$. The matched sensitivity into an open load is given by [2]

$$\beta_{V,opt} = \frac{R_J\gamma/2}{\left(1+R_S/R_J\right)\left(1+R_S/R_J+\left(2\pi fC_J\right)^2 R_S R_J\right)} \quad (1)$$

S_{11} can also be written in terms of a lengthy combination of the model parameters. Figure 3 plots the unmatched sensitivity versus frequency data with the model curve obtained by substituting for $\beta_{V,opt}$ and S_{11}. Note that the sensitivity values themselves are not used in the parameter fitting. Excellent agreement between measurement and simulation is obtained for the diodes with areas above

2x2 μm^2. The simulation for the 2x2 μm^2 diodes rolls off slightly faster with frequency than the measured values indicate. Better agreement at the higher frequencies may depend on more accurate knowledge of the nature of the diode contacts. There seems to be an instrumental discrepancy at 30 GHz for the two smaller diodes. A check of the sensitivity versus input power level shows that the 2x2 μm^2 diode obeys the square law dependence up to about -15 dBm.

OPTIMAL SENSITIVITY MEASUREMENTS

At low frequency, and ignoring R_S relative to R_J, Eq. 1 reduces to $\beta_{V,opt} \approx R_J \gamma / 2$. At high frequency the frequency term in the denominator dominates and $\beta_{V,opt} \approx \gamma / 8 (\pi f C_J)^2 R_S$. The frequency dividing these two regimes is $f_D = 1/2\pi\sqrt{R_S R_J C_J^2}$. The limits show that R_J is critical for obtaining large $\beta_{V,opt}$ in the low frequency regime, whereas R_S and C_J are more important for high frequencies. Since C_J should be proportional to area, and R_S should be proportional to inverse area or less, it is clear that decreasing the diode area will lead to further enhancement of the frequency response.

S_{11} has the simple low frequency limit $S_{11} \approx (R_J+R_S-50\Omega)/(R_J+R_S+50\Omega)$. Substituting this in β_V and taking the further limits that usually $R_J >> 50\Omega$ and $R_J >> R_S$ produces the very simple low frequency estimate $\beta_V \approx 100 \times \gamma$, in Volts/Watts. The low frequency data points of Fig. 3 are consistent with the value of γ=28.0/Volt for SB2775. This gives additional confidence that the low frequency estimate for the optimal sensitivity, $\beta_{V,opt} \approx R_J \gamma /2$, is applicable for $f < f_D$. For example, an R_J of 10,000Ω would yield an optimal sensitivity of about 10,000×28/2=140,000 (V/W).

Table 1, last column, gives an estimate for the optimal sensitivity at 95 GHz. This is well beyond f_D which ranges from 15 to 25 GHz. Thus the optimal sensitivity is decreasing approximately as $1/f^2$. The $\beta_{V,opt}$ estimate is obtained from the measured sensitivity value in the adjacent column enhanced by the directly measured reflection coefficient. S_{11} is related to Z_D by $S_{11}=(Z_D-50\Omega)/(Z_D+50\Omega)$. The 2x2 μm^2 diodes are seen to have optimal sensitivities of about 7000 V/W.

CONCLUSIONS

The high sensitivity, low cost, and reproducibility of this new diode indicate that it will find a variety of usages where zero bias direct detection is required. The flexibility of independent barrier width and diode area control of R_J provides the ability to optimize among several possible desired properties, including low or high frequency sensitivity, dynamic range, square law linearity, noise, bandwidth, temperature sensitivity, etc. We would like to acknowledge essential technical discussions with John Lovberg of Trex Enterprises.

REFERENCES

(1) J. N. Schulman and D. H. Chow, "Sb-heterostructure interband backward diodes," IEEE Electron Device Letters **21**, pp. 353-355, July 2000.

(2) I. Bahl and P. Bhartia, Microwave Solid State Circuit Design, John Wiley and Sons, New York, 1988, ch. 11.

(3) P. Fay, Lu Jiang, Y. Xu, G. H. Bernstein, D. H. Chow, J. N. Schulman, H. L. Dunlap, and H. J. De Los Santos, "Fabrication of monolithically integrated InAlAs/InGaAs/InP HEMTs and InAs/AlSb/GaSb resonant interband tunneling diodes", IEEE Trans. Electron Devices **48**, pp. 1282-1284, June 2001.

(4) J. Steinshnider, M. Weimer, R. Kaspi, and G. W. Turner, "Visualizing interfacial structure at non-common-atom heterojunctions with cross-sectional scanning tunneling microscopy", Phys. Rev. Lett. **85**, pp. 2953-2956, October 2000. Also, see references 6-14 therein.